HHS Public Access

Author manuscript

J Biomech. Author manuscript; available in PMC 2016 February 09.

Published in final edited form as:

J Biomech. 2014 June 27; 47(9): 2070–2079. doi:10.1016/j.jbiomech.2014.03.011.

Characterization of Evolving Biomechanical Properties of Tissue Engineered Vascular Grafts in the Arterial Circulation

Brooks V. Udelsman[*], **Ramak Khosravi**[*], **Kristin S. Miller**[†], **Ethan W. Dean**[*], **Matthew R. Bersi**[†], **Kevin Rocco**[†], **Tai Yi**[‡], **Jay D. Humphrey**[†], and **Christopher K. Breuer**[‡]

[*]Yale University School of Medicine, 10 Amistad Street New Haven, CT 06519, USA

[†]Yale School of Engineering and Applied Science, 55 Prospect Street, New Haven, CT 06520, USA

[‡]Nationwide Children's Hospital, 700 Children's Drive-WB4151, Columbus, OH 43205 USA

Abstract

We used a murine model to assess the evolving biomechanical properties of tissue engineered vascular grafts (TEVGs) implanted in the arterial circulation. The initial polymeric tubular scaffold was fabricated from (poly)lactic acid (PLA) and coated with a 50:50 copolymer of (poly)caprolactone and (poly)lactic acid (P[PC/LA]). Following seeding with syngeneic bone marrow derived mononuclear cells, the TEVGs (n=50) were implanted as aortic interposition grafts in wild-type mice and monitored serially using ultrasound. A custom biaxial mechanical testing device was used to quantify *in vitro* the circumferential and axial mechanical properties of grafts explanted at 3 or 7 months. At both times, the TEVGs were much stiffer than native tissue in both directions. Repeat mechanical testing of some TEVGs treated with elastase or collagenase suggested that elastin did not contribute significantly to the overall stiffness whereas collagen did contribute. Traditional histology and immunostaining revealed smooth muscle cell layers, significant collagen deposition, and increasing elastin production in addition to considerable scaffold at both 3 and 7 months, which likely dominated the high stiffness seen in mechanical testing. These results suggest that PLA has inadequate *in vivo* degradation, which impairs cell-mediated development of vascular neotissue having properties closer to native arteries. Assessing contributions of individual components, such as elastin and collagen, to the developing neovessel is needed to guide computational modeling that may help to optimize the design of the TEVG.

Keywords

Tissue engineering; mechanical homeostasis; neovascularization; growth and remodeling

Corresponding Author: Christopher K. Breuer, MD, 700 Children's Drive – WB4151, Columbus, Ohio 43205, Phone: (614) 355-5754, Christopher.Breuer@NationwideChildrens.org.

Conflict of Interest Statement

We have no other conflicts of interest to report.

Introduction

Arteries respond to changes in mechanical loading through a process of growth (changes in mass) and remodeling (changes in structure) that tends to maintain nearly constant the mechanical environment experienced by the cells. Termed —mechanical homeostasis, the associated mechanobiological responses occur at multiple levels, from whole tissue down to cellular and subcellular structures (Humphrey, 2008). For example, large arteries regulate their lumen via endothelial cell – smooth muscle cell responses that maintain a wall shear stress of ~ 1.5 Pa in humans (Greve et al., 2006). Indeed, even pathologic situations such as aneurysms, which alter the hemodynamic loading, result in a significant remodeling of extracellular matrix, via increased matrix metalloproteinase (MMP) activity and synthesis of collagens type I and III, that again appears to seek to return wall stresses toward normal levels (Kassam et al., 2004; Peters et al., 2001).

The mechanobiology of neotissue formation has not been well explored in the field of vascular tissue engineering, wherein the focus is generally on gross mechanical metrics (e.g., burst pressure) or the molecular biology (e.g., cytokine activity) independent of mechanical stimuli. Because a degradable polymeric scaffold, such as a tissue engineered vascular graft (TEVG), can exhibit changing mechanical properties, as well as change the hemodynamics and the axial loads acting on the host vessels, there is a pressing need to correlate the evolving cell and matrix biology with the evolving mechanics. Indeed, the radical change in mechanical environment introduced by an interpositional TEVG necessitates evaluation of the adaptive response of the adjacent artery.

An understating of the mechanobiology of native arteries has led to the development of computational models that predict salient features of arterial growth and remodeling (G&R) in response to changes in blood pressure, flow, and axial loading (Baek et al., 2006; Gleason and Humphrey, 2005). Recently, this G&R framework has been used to simulate TEVGs grown in bioreactors (Niklason et al., 2010) and those used as venous interposition grafts (Miller et al., 2013). As of yet, however, there is insufficient experimental data with which to generate computational models for TEVGs implanted within the arterial circulation. Were such models to be developed, they could be a powerful allied tool, allowing for refinement and optimization of TEVG design *in silico* prior to more time intensive *in vivo* studies. Herein, we report the first characterization of evolving biomechanical properties of implanted TEVGs in the arterial circulation of a murine model. Our objective was twofold: to evaluate the evolving mechanical features of arterial TEVGs and to begin to collect the experimental data needed for building computational models of G&R for tissue engineering applications.

Methods

Graft Fabrication, Implantation, and Monitoring

TEVG scaffolds were constructed from sheets of nonwoven (poly)lactic acid (PLA; Concordia Fibers, Coventry, RI) that were rolled into a tube and sealed with a 50:50 copolymer of ε-(poly)caprolactone and L-(poly)lactide (P[PC/LA]; Absorbable Polymers International, Birmingham, AL) as described previously (Roh et al., 2008). Scaffolds were

~3.5 mm long, with an inner diameter of ~700 μm and wall thickness of ~ 290 μm (Fig. 1). Given our current methods of fabrication, these dimensions were the smallest that yielded consistent scaffolds.

The Institutional Animal Care and Use Committee at Yale University approved all animal procedures. Prior to implantation of the graft, bone marrow derived mononuclear cells (BM-MNCs) were harvested from the tibia, femur, and humerus of 8–10 week old male C57BL/6 mice and isolated via density-gradient centrifugation using histopque-1077 (Sigma). The isolated cells were used to statically seed the scaffolds (~1×10^6 cells/scaffold) as described previously (Roh et al., 2010). The cell-seeded TEVGs were implanted as interpositional grafts in the infrarenal abdominal aorta (IAA) in 50 female CB57BL/6 mice between 8 and 10 weeks of age; this procedure was accomplished using a sterile microsurgical technique (Roh et al., 2008). TEVG patency, wall thickness, and luminal diameter were assessed *in vivo* using high frequency ultrasound system (Vevo 770, Visualsonics, Toronto, Canada) with an RMV-704 transducer.

Mechanical Testing

TEVGs were harvested for biaxial mechanical testing at 3 and 7 months. Following anesthesia using a peritoneal injection of ketamine and xylazine, a continuous vascular segment was harvested containing the TEVG as well as native IAA both proximally and distally. Prior to explant, India ink was use to mark the proximal IAA, proximal TEVG, distal TEVG, and distal IAA. In order to ensure adequate pressurization and to prevent leakage during *in vitro* testing, branching vessels were identified and ligated. Photographs were taken to record the positions of the ink marks before explant and 10 minutes thereafter. Distances between marks were calculated with ImageJ software and used to determine the ratio between loaded and unloaded length, also known as *in vivo* axial stretch. After explant, the composite vessel was cannulated and secured to custom drawn micropipettes with 6-0 suture. The cannulated vessels were placed within a custom computer-controlled biaxial testing device (Gleason et al., 2004). The testing chamber was filled with a physiologic buffered solution (PBS), including calcium chloride and magnesium chloride (Hank's; Gibco, Inc.) (Fig. 2).

The composite vessels (proximal IAA—TEVG—distal IAA) were placed within the device at their unloaded state and initial unloaded dimensions were recorded. Prior to testing, vessels were allowed to equilibrate at 80 mmHg for 15 minutes at their measured *in vivo* axial stretch. The vessels were then preconditioned at this axial stretch by 4 cycles of pressurization from 10 to 100 mmHg at a rate of ~2 mmHg/second. Following preconditioning, unloaded dimensions were measured again; increases in dimensions relative to those taken prior to preconditioning and equilibration were minimal. The *in vivo* axial stretch of the composite vessel was also estimated *in vitro* by identifying the axial stretch at which axial force remained nearly constant in response to changes in luminal pressure (Ferruzzi et al., 2013a). This estimation was accomplished by measuring axial force at pressures of 50 mmHg, 60 mmHg, 80 mmHg, and 100 mmHg at axial stretches slightly above and below the value of axial stretch measured from the India ink dots. With the camera focused on the central region of the TEVG, pressure-diameter testing consisted of

cyclic pressurization from 10 to 100 mmHg at the experimentally determined *in vivo* axial stretch and at ±5% this value. Pressure-diameter testing was repeated with the camera focused on the proximal IAA. Luminal pressure, axial force, outer diameter, and overall axial length were measured continually throughout testing using a custom LabView program.

In a sub-set of specimens, the composite vessel, containing proximal IAA, TEVG, and distal IAA, was perfused with either collagenase (1035 U/ml; Worthington Biochemical Corporation) or elastase (7.5 U/ml; Worthington Biochemical Corporation) while at the experimentally determined *in vivo* axial stretch and maintained at 5mmHg and 80 mmHg, respectively. Consistent with prior studies (Collins et al., 2012), the collagenase, having a brown tint, remained intraluminal until collagen degradation allowed slow leaking from the IAA into the bath (after ~20 minutes). At this point the mechanical integrity of the native IAA was compromised, but the TEVG could still be pressurized. The TEVG was thus isolated immediately from the IAA, cannulated, washed with PBS, and subjected again to cyclic pressure-diameter testing at its original *in vivo* axial stretch though a pressure range of 10 to 100 mmHg. In contrast, consistent with prior studies (Ferruzzi et al., 2011; Collins et al., 2012), the elastase perfusion was maintained for 30 minutes without any leakage, after which the dilatation of the proximal and distal IAA reached steady state and the remaining elastase was washed out with PBS. Pressure-diameter testing was performed again on the composite vessel (i.e., TEVG and proximal IAA) at the original *in vivo* axial stretch and ±5% this value.

Histology and Immunohistochemistry

Samples explanted at 3 and 7 months were fixed in 10% neutral buffered formalin for 24 hours and embedded in paraffin (Roh et al., 2010). Samples were stained with hematoxylin and eosin (H&E), Masson's Trichrome (TRI), picrosirius red (PSR), Movat's Pentachrome (MOV), and Verhoeff-Van Gieson (VVG). VVG and TRI stained samples were analyzed with a custom Matlab code that quantifies pixels associated with elastin and collagen, respectively. A similar program was used to calculate the relative distribution of large and small collagen fibers on PSR-stained sections. Unstained samples used for immunohistochemistry (IHC) were rehydrated and blocked for endogenous peroxidase activity; antibodies included those for CD31 (endothelial cell marker; Abcam), α-smooth muscle actin (Dako), calponin (Abcam), F4/80 (marker for mouse macrophages; AbD Serotec), MMP-2 (Abcam), MMP-9 (Abcam), collagen type I (Abcam), and collagen type III (Abcam). Antibody binding was detected using biotinylated secondary antibodies, followed by binding of streptavidin horseradish peroxidase (Naito et al., 2012). For immunofluorescence detection, tropoelastin (elastin marker; Abacam) was used with subsequent 4′,6-diamidino-2-phenylindole nuclear counterstaining (Roh et al., 2010).

Statistical Analysis

Pressure-diameter curves were normalized by dividing all outer diameter measurements by the minimum diameter at a given axial stretch and presented as mean ± standard error of the mean (SEM). All other data were represented as mean ± standard deviation (SD). Ultrasound data collected at multiple times were analyzed by using two-way analysis of

variance (ANOVA) with repeated measures, followed by Sidak's multiple comparisons test. All other comparisons between groups were performed using either a Student's t-test or one-way ANOVA, followed by Tukey's multiple comparisons test. P-values < 0.05 were considered statistically significant.

Results

In vivo monitoring

Fourteen of the fifty mice implanted (28%) were euthanized or died prematurely due to graft related complications (Fig. 3 *a*, *b*). Three distinct periods of failure were observed: Early, within hours post-implant due to complications of micro-surgery (2%); Intermediate, between 5 and 14 days due to failure of the P[PC/LA] sealant with resulting rupture along the seam on the scaffold (18%); and Late, between 14 days and 42 days due to rupture of the wall of the TEVG (8%). No graft related mortality occurred after 42 days and overall survival was 72%. On Doppler ultrasound, surviving mice had a larger luminal diameter within the TEVG when compared to native aorta, consistent with the use of over-sized grafts (i.e., grafts were ~680 μm in diameter at implantation relative to a native aortic diameter of ~430μm). Wall thickness of the TEVGs also remained significantly greater than that of the native aorta consistent with its initially larger thickness (290 μm). Over the experimental time course, the TEVGs demonstrated stability in both luminal diameter and wall thickness without any statistically significant changes between 2 and 24 weeks (Fig. 3). Surviving TEVGs did not become stenotic or have intraluminal thrombus.

TEVGs exhibited high structural stiffness

The TEVGs had significantly lower values of axial stretch than the IAA at both 3 and 7 months, with no differences between these times (Fig. 4 *a* and *b*). Pressure-diameter curves of mounted composite vessels demonstrated a lack of compliance in the TEVGs compared with proximal IAA over a pressure range of 10 to 100 mmHg at both times (Fig. 5). Note, that the composite vessel maintained nearly constant axial force during pressure-diameter testing at the experimentally determined *in vivo* axial stretch (Fig. 4*c*).

TEVGs developed smooth muscle layers and an endothelial cell lining

Histology confirmed that the TEVGs had an increased luminal diameter and wall thickness relative to native IAA harvested from aged-matched controls (Fig. 6). The difference in luminal area appeared more pronounced on histologic staining than on ultrasound, likely due increased recoil and dehydration effects during fixation in the native tissue. H&E staining showed abundant residual polymer at both times, particularly when viewed under polarized light due to the innate birefringence of PLA (cf. Fig. 8*r*). Immuno-staining revealed that there was extensive cellular infiltration within the TEVGs (Fig. 6), with positive staining for calponin and α-smooth muscle actin indicating smooth muscle cells. Note that the calponin was mainly in concentric neotissue layers between the polymer and endothelialized lumen, the latter of which was revealed by positive staining for CD31. The presence of extensive macrophages on F4/80 staining suggested an inflammatory component to the remodeling process, which was further characterized by the positive staining of MMP-2 and MMP-9 at 3 months. MMP-2 staining persisted at 7 months, when MMP-9 was decreased (Fig. 7).

Collagen contributed to TEVG stiffness

Extensive deposition of collagen was demonstrated by TRI staining (Fig 8). Quantification of pixels positive for the collagen revealed similar area fractions for collagen between native IAA and TEVG at both 3 and 7 months. PSR, which provides information on the diameter of the collagen fibers, revealed a similar pattern of distribution of large (red/orange) and small (yellow/green) collagen fibers between native IAA and TEVG at both low and high light exposure (Fig. 8). The low light exposure was used to focus on the adventitia, while the high light exposure was used to focus on the media. Collagen content of TEVGs was further characterized by immunostaining, which revealed collagen type I (COL I) and collagen type III (COL III) throughout the TEVG wall, closely associated with areas containing residual polymer.

Whereas complete enzymatic degradation of collagen caused the TEVG to leak, partial treatment with collagenase maintained structural integrity. Pressure-diameter testing at 3 and 7 months demonstrated a modest increase in TEVG compliance due to partial loss of collagen, hence implying some contribution of collagen to the circumferential stiffness that was dominated by polymer post-treatment (Fig. 9).

Elastin did not contribute to TEVG stiffness

By 3 months, elastin was evident along the inner circumferential layers of the TEVG (Fig. 10). Using a digital extraction method and VVG staining, we found a significant increase in the area fraction of elastin between 3 and 7 months. Nevertheless, the elastin fraction was significantly lower than native at both times. In addition, the elastic fibers in the TEVG appeared thinner and less organized than those in native tissue, most notably on immune-staining of tropoelastin (Fig. 10). Treatment with elastase did not significantly change TEVG compliance at 3 or 7 months (Fig. 9). Conversely, the elastase did decrease the compliance of the proximal IAA, which then mimicked the appearance of the TEVG pressure-diameter curves.

Discussion

Vascular neotissue formation describes the process by which a biodegradable scaffold transforms into a living vascular conduit, whether initially seeded with cells or not. As the scaffold degrades, neotissue forms and ultimately gives rise to a neovessel when the scaffolding is degraded completely. Despite significant advances in our understanding of mechanobiological factors affecting vascular biology in health and disease, there has been little research on these processes during neovessel formation. The biomechanical properties of the TEVG are initially determined exclusively by the properties of the tubular scaffold, but over time the cells begin to produce an extracellular matrix that increasingly contributes to the properties of the graft. As in native blood vessels, this extracellular matrix is composed primarily of collagen, elastin, and glycosaminoglycans. As the scaffold degrades, it is thought that the cells can sense the increased load borne by the deposited extracellular matrix, which it presumably remodels in an attempt to establish the aforementioned mechanical homeostasis. At the point when the scaffold degrades completely, the extracellular matrix is necessarily the primary determinant of the biomechanical properties

of the graft and hence both the overall structural integrity and adaptive potential. Recent work by Naito, Lee and colleagues demonstrated that developing venous TEVGs composed of an initially stiff (poly)glycolic acid (PGA) scaffold develop increased compliance that approaches native IVC by 24 weeks after implantation (Naito et al., 2013). They suggest a complex, time-dependent process in which collagen deposited during the first 12 weeks is replaced or remodeled into more compliant forms in the context of a fully degraded PGA scaffold. See, too, the associated modeling study that captures salient aspects of the associated biomechanics (Miller et al., 2013).

The present study was designed to determine if similar mechanobiological processes occur in neovessel formation within the arterial system and to generate mechanical data to serve as a foundation for the extension of the prior computational modeling to the arterial system. We found that, despite initial mortality associated with seam line rupture, PLA-based TEVGs were stable after 6 weeks with no aneurysmal dilation, stenosis, or intraluminal thrombosis up to 7 months. Similar to prior reports (Mirensky et al., 2009), these TEVGs developed a luminal endothelial cell layer as well as a smooth muscle cell populated — medial layer. Structurally, our results revealed many of components of a normal extracellular matrix, including elastin and collagen types I and III (Wagenseil and Mecham, 2009). MMP-2 and MMP-9 activity, along with extensive infiltration by macrophages, suggested an ongoing inflammatory mediated process of remodeling. This chronic inflammation likely resulted from the persistence of the PLA, which contributed to the continued stiffness in both the circumferential and axial directions. The elastin found histologically played no mechanical role in overall TEVG performance while the collagen contributed only moderately to the stiffness. Hence, although the graft satisfied minimal mechanical requirements, such as sufficient suture retention and burst pressure, and clinical requirements, such as lack of stenosis or aneurysmal expansion, it clearly had not approached native structure or function by 7 months.

Our work can be contrasted with a recent study in which TEVGs composed of an inner layer of (poly)glycerol sebacate (PGS) and an outer sheath of (poly)caprolactone (PCL) were implanted in the IAA of a rat for up to 3 months (Wu et al., 2012). In contrast to the present findings, the PGS degraded rapidly and was replaced entirely with new matrix while remnants of the PCL sheath persisted over the study period. The associated TEVG exhibited considerable material compliance, with circumferential Cauchy stresses on the order of 40 kPa compared with those of order 120 kPa for native at comparable levels of strain. Overall (circumferential) compliance was similar to native and this approach engenders considerable promise. From the perspective of developing a data-driven computational model for hypothesis testing, it would be advantageous to compare directly the data from the present TEVG (structurally too stiff) and that based on the PGS/PCL (materially too compliant) as we continue to search for the optimal combination of scaffold properties, including initial stiffness and rate of degradation.

Not only are the properties of a TEVG important for its integrity and adaptivity, they are also important determinants of mechanobiological adjustments by the adjacent host vessels. Toward this end, we observed a persistent compensation by the native IAA in response to the high stiffness of the TEVG. At the composite vessel's *in vivo* axial stretch, a near

constant force could be achieved through a range of pressures, similar to that of native arteries in the preferred homeostatic state (Humphrey et al., 2009). Yet, the axial force in the composite vessels was lower by ~4 mN compared with the axial force in non-implanted IAA in C57BL/129sv mice (Ferruzzi et al., 2013b); likewise, there was a decreased compliance in the proximal IAA relative to normal (Fig. 11). Although differences in mouse backgrounds (pure versus mixed C57BL/6) and testing procedures (e.g., pressurization up to 100 mmHg rather than 140 mmHg) may have contributed to the observed differences, both differences seen in Fig. 11 likely resulted from the adjacent host aorta adapting to the stiff interpositional TEVG. Optimal design of TEVGs should clearly seek to minimize adverse adaptations in the host vessels.

This study was the first to examine long-term changes in the structure and mechanical properties of TEVGs in the murine arterial system. Despite the technical challenges of implanting interpositional grafts in such small arteries, the availability of so many genetically modified mouse models necessitates such an approach. Our current methods of fabrication resulted in an over-sized graft, but this would be expected to affect the blood flow, not the blood pressure within the TEVG. Given that the pressure, and the associated intramural stresses, appear to dominate intramural remodeling, this technical limitation was acceptable. Indeed, because of the absence of intraluminal thrombus, the disturbance in blood flow was likely not critical either. There is, nonetheless, a need to scale-down our fabrication methods to yield appropriately sized grafts for the mouse, particularly ones having near native wall thickness since thickness contributes directly to structural stiffness. In conclusion, the present data highlight the need to evaluate mechanically the separate contributions of different matrix components to overall stiffness, for the mere presence of significant matrix need not imply significant load carrying capability, and the need to assess possible adaptive responses by the adjacent host tissue, which can in turn provide mechanobioloical cues to the cells developing the neotissue. Finally, it is hoped that such data can inform computational models that accelerate the search for preferred time courses of polymer degradation and matrix incorporation with an evolving graft. Only in this way can we move beyond purely trial and error experimental approaches to improving tissue engineered vessels and open the door for next generation rationally designed TEVGs.

Acknowledgments

This research was supported, in part, by a Medical Student Fellowship from the Howard Hughes Medical Institute (B. Udelsman) as well as grants from the NIH: R01-HL098228 (C. Breuer) and 5T32-HL098069 (A. Sinusas). We would also like to acknowledge Angela Huang and the laboratory of L. Niklason for help with the immunofluorescence imaging.

References

Baek S, Rajagopal KR, Humphrey JD. A theoretical model of enlarging intracranial fusiform aneurysms. Journal of biomechanical engineering. 2006; 128:142–149. [PubMed: 16532628]

Collins MJ, Eberth JF, Wilson E, Humphrey JD. Acute mechanical effects of elastase on the infrarenal mouse aorta: implications for models of aneurysms. Journal of biomechanics. 2012; 45:660–665. [PubMed: 22236532]

Ferruzzi J, Bersi MR, Humphrey JD. Biomechanical Phenotyping of Central Arteries in Health and Disease: Advantages of and Methods for Murine Models. Annals of biomedical engineering. 2013a

Ferruzzi J, Bersi MR, Humphrey JD. Biomechanical phenotyping of central arteries in health and disease: advantages of and methods for murine models. Annals of biomedical engineering. 2013b; 41:1311–1330. [PubMed: 23549898]

Ferruzzi J, Collins MJ, Yeh AT, Humphrey JD. Mechanical assessment of elastin integrity in fibrillin-1-deficient carotid arteries: implications for Marfan syndrome. Cardiovascular research. 2011; 92:287–295. [PubMed: 21730037]

Gleason RL, Gray SP, Wilson E, Humphrey JD. A multiaxial computer-controlled organ culture and biomechanical device for mouse carotid arteries. J Biomech Eng. 2004; 126:787–795. [PubMed: 15796337]

Gleason RL, Humphrey JD. Effects of a sustained extension on arterial growth and remodeling: a theoretical study. Journal of biomechanics. 2005; 38:1255–1261. [PubMed: 15863110]

Greve JM, Les AS, Tang BT, Draney Blomme MT, Wilson NM, Dalman RL, Pelc NJ, Taylor CA. Allometric scaling of wall shear stress from mice to humans: quantification using cine phase-contrast MRI and computational fluid dynamics. American journal of physiology Heart and circulatory physiology. 2006; 291:H1700–1708. [PubMed: 16714362]

Humphrey JD. Vascular adaptation and mechanical homeostasis at tissue, cellular, and sub-cellular levels. Cell biochemistry and biophysics. 2008; 50:53–78. [PubMed: 18209957]

Humphrey JD, Eberth JF, Dye WW, Gleason RL. Fundamental role of axial stress in compensatory adaptations by arteries. Journal of biomechanics. 2009; 42:1–8. [PubMed: 19070860]

Kassam AB, Horowitz M, Chang YF, Peters D. Altered arterial homeostasis and cerebral aneurysms: a molecular epidemiology study. Neurosurgery. 2004; 54:1450–1460. discussion 1460–1452. [PubMed: 15157303]

Miller KS, Lee YU, Naito Y, Breuer CK, Humphrey JD. Computational model of the in vivo development of a tissue engineered vein from an implanted polymeric construct. Journal of biomechanics. 2013

Mirensky TL, Nelson GN, Brennan MP, Roh JD, Hibino N, Yi T, Shinoka T, Breuer CK. Tissue-engineered arterial grafts: long-term results after implantation in a small animal model. J Pediatr Surg. 2009; 44:1127–1132. discussion 1132–1123. [PubMed: 19524728]

Naito Y, Lee YU, Yi T, Church SN, Solomon D, Humphrey JD, Shinoka T, Breuer CK. Beyond Burst Pressure: Initial Evaluation of the Natural History of the Biaxial Mechanical Properties of Tissue Engineered Vascular Grafts in the Venous Circulation Using a Murine Model. Tissue engineering. Part A. 2013

Naito Y, Williams-Fritze M, Duncan DR, Church SN, Hibino N, Madri JA, Humphrey JD, Shinoka T, Breuer CK. Characterization of the natural history of extracellular matrix production in tissue-engineered vascular grafts during neovessel formation. Cells, tissues, organs. 2012; 195:60–72. [PubMed: 21996715]

Niklason LE, Yeh AT, Calle EA, Bai Y, Valentin A, Humphrey JD. Enabling tools for engineering collagenous tissues integrating bioreactors, intravital imaging, and biomechanical modeling. Proc Natl Acad Sci U S A. 2010; 107:3335–3339. [PubMed: 19955446]

Peters DG, Kassam AB, Feingold E, Heidrich-O'Hare E, Yonas H, Ferrell RE, Brufsky A. Molecular anatomy of an intracranial aneurysm: coordinated expression of genes involved in wound healing and tissue remodeling. Stroke; a journal of cerebral circulation. 2001; 32:1036–1042.

Roh JD, Nelson GN, Brennan MP, Mirensky TL, Yi T, Hazlett TF, Tellides G, Sinusas AJ, Pober JS, Saltzman WM, Kyriakides TR, Breuer CK. Small-diameter biodegradable scaffolds for functional vascular tissue engineering in the mouse model. Biomaterials. 2008; 29:1454–1463. [PubMed: 18164056]

Roh JD, Sawh-Martinez R, Brennan MP, Jay SM, Devine L, Rao DA, Yi T, Mirensky TL, Nalbandian A, Udelsman B, Hibino N, Shinoka T, Saltzman WM, Snyder E, Kyriakides TR, Pober JS, Breuer CK. Tissue-engineered vascular grafts transform into mature blood vessels via an inflammation-mediated process of vascular remodeling. Proc Natl Acad Sci U S A. 2010; 107:4669–4674. [PubMed: 20207947]

Wagenseil JE, Mecham RP. Vascular extracellular matrix and arterial mechanics. Physiological reviews. 2009; 89:957–989. [PubMed: 19584318]

Wu W, Allen RA, Wang Y. Fast-degrading elastomer enables rapid remodeling of a cell-free synthetic graft into a neoartery. Nature medicine. 2012; 18:1148–1153.

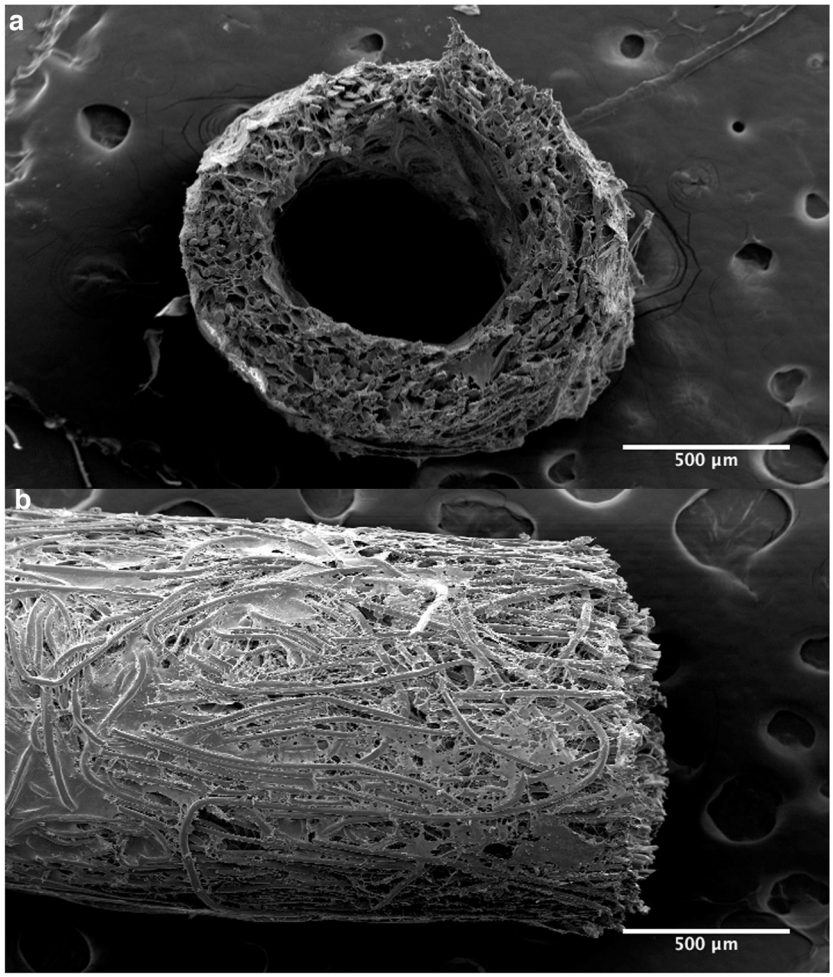

Figure 1.

Scanning electron microscopic image of a representative pre-implant TEVG showing both a cross-sectional (*a*) and a longitudinal (*b*) section.

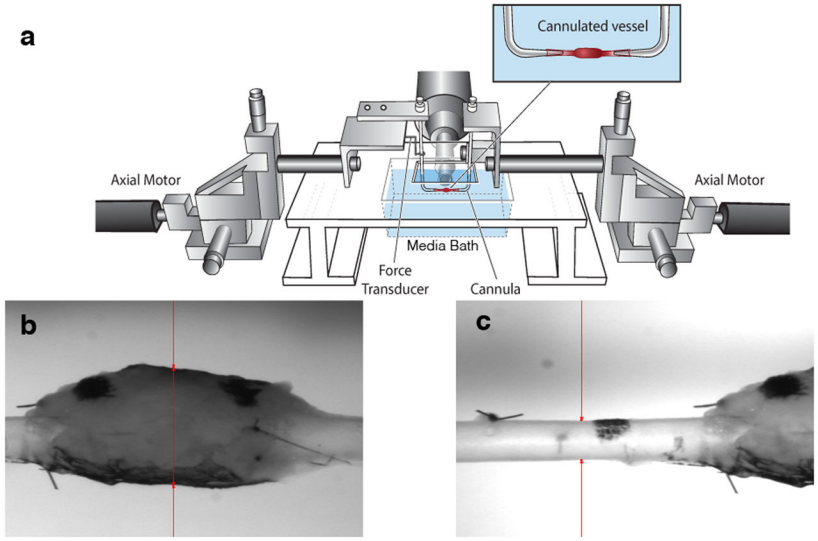

Figure 2.

Schematic drawing of the biaxial mechanical testing device. (*a*) The composite vessel, consisting of the proximal IAA-TEVG-distal IAA, was cannulated using custom micropipettes. Luminal flow and pressure were controlled through the micropipettes and axial stretch was controlled via paired stepper motors; pressure and force were monitored with standard transducers. (*b*) Representative image of a TEVG mounted within the device with the video camera used for measuring diameter focused on the TEVG. (*c*) Representative image of a TEVG within the device with the camera focused on the proximal IAA. Outer diameter is indicated by the red arrows.

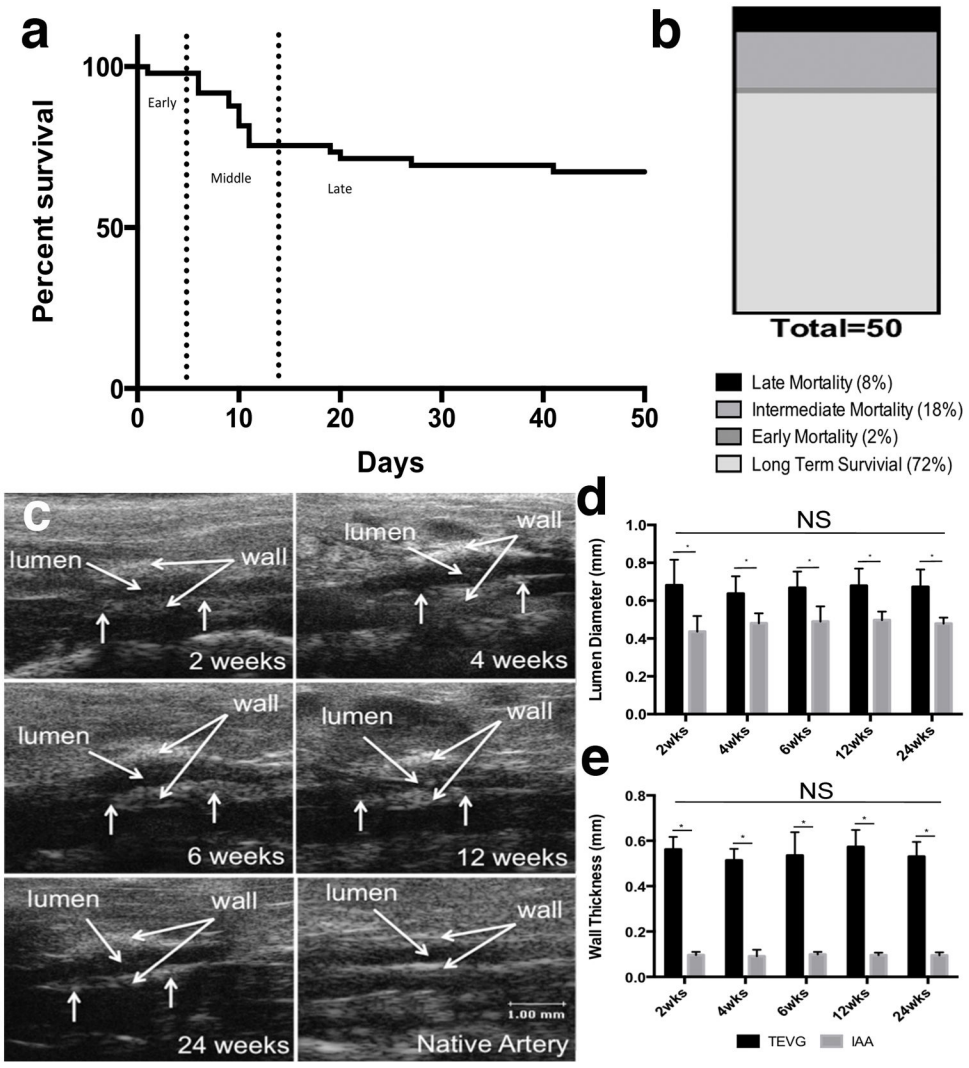

Figure 3.

Survival and *in vivo* evaluation of TEVGs. (*a*) Survival curve demonstrating three distinct periods of mortality: early, intermediate, and late. (*b*) Percentage of long-term survival and mortality. (*c*) Representative Doppler ultrasound images of TEVGs at various times, which show consistent graft patency. (*d*) TEVG luminal diameter as measured by Doppler ultrasound (*n*=12). (*e*) TEVG wall thickness as measured by Doppler ultrasound (*n* =12). Data in graphs are expressed as mean ± SD.

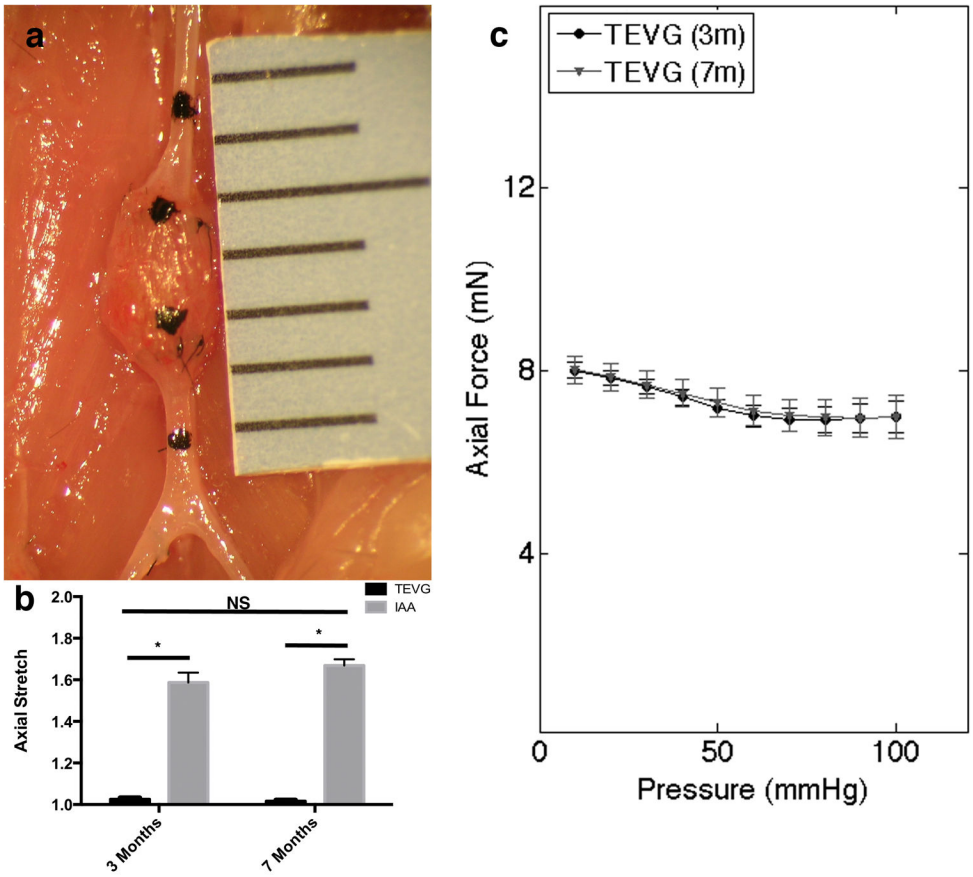

Figure 4.

Evaluation of axial stretch and force. (*a*) Representative image of TEVG at explant. Note: India ink marked proximal IAA, proximal TEVG, distal TEVG, and distal IAA. (*b*) Axial stretch ratio of the loaded and unloaded state measured at 3 (*n*=9) and 7 (*n*=6) months expressed as mean ± SD. (*c*) Axial Force during pressure-diameter curves at 3 and 7 months at *in vivo* axial stretch expressed as mean ± SEM.

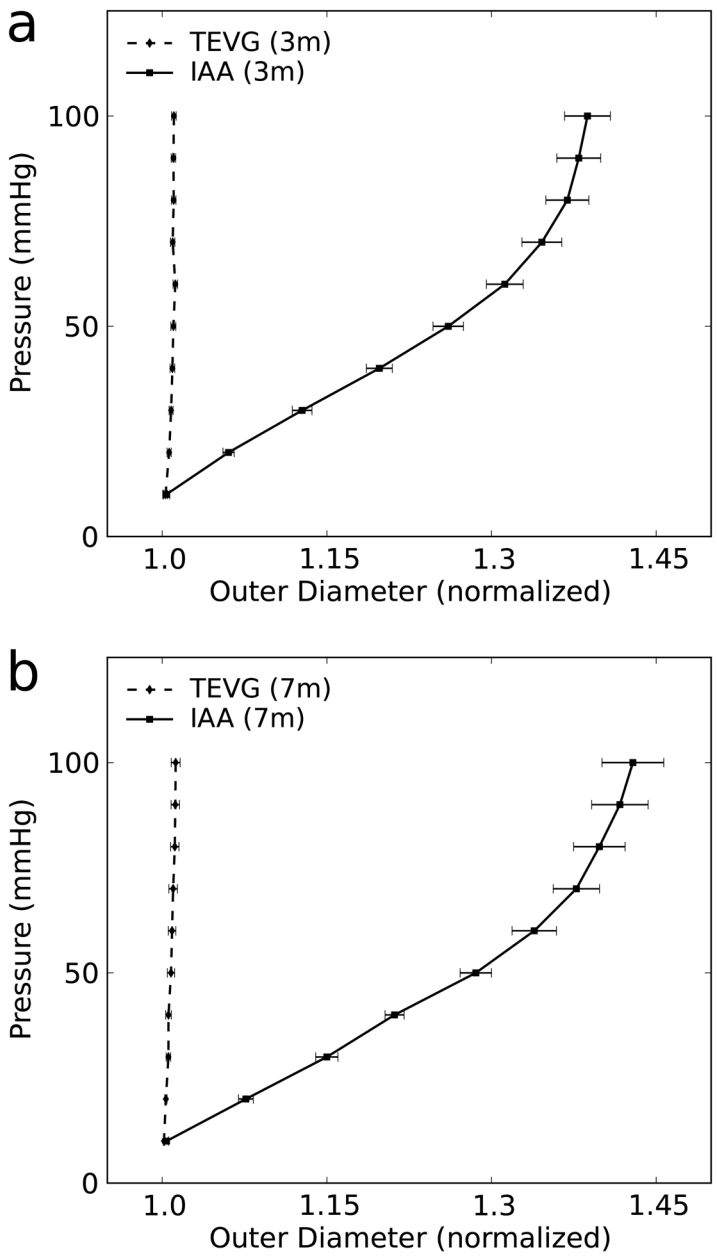

Figure 5.

Pressure-diameter curves at (*a*) 3 months (*n*=9) and (*b*) 7 months (*n*=6) comparing proximal IAA and TEVG at *in vivo* axial stretches. Data in graphs are expressed as mean ± SEM.

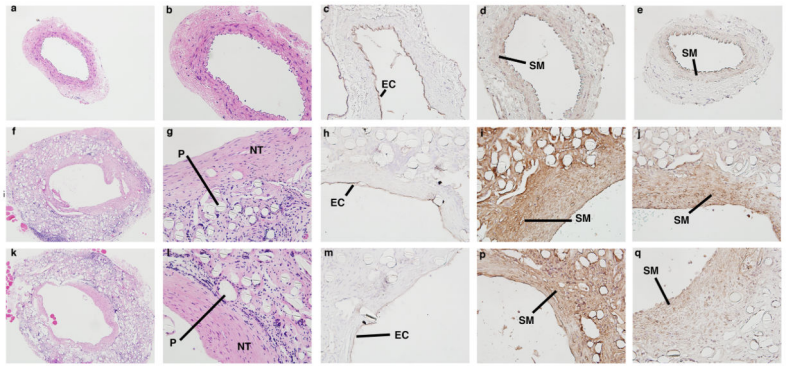

Figure 6.

Morphologic evaluation of mouse IAA and TEVG at 3 and 7 months post-implantation. Native mouse IAA stained for (*a*–*e*): H&E (cell nuclei), CD31 (endothelial cells (EC)), and SMA and CAL (smooth muscle (SM)). Similarly, TEVG at 3 months (*f*–*j*) and 7 months (*k*–*q*) stained for: H&E, CD31, SMA, and CAL. Note the abundant residual polymer (P) in the TEVG, with the neotissue (NT) forming along the lumen. Low-magnification photomicrographs are at magnification of 50×. All other photomicrographs are at a magnification of 200×.

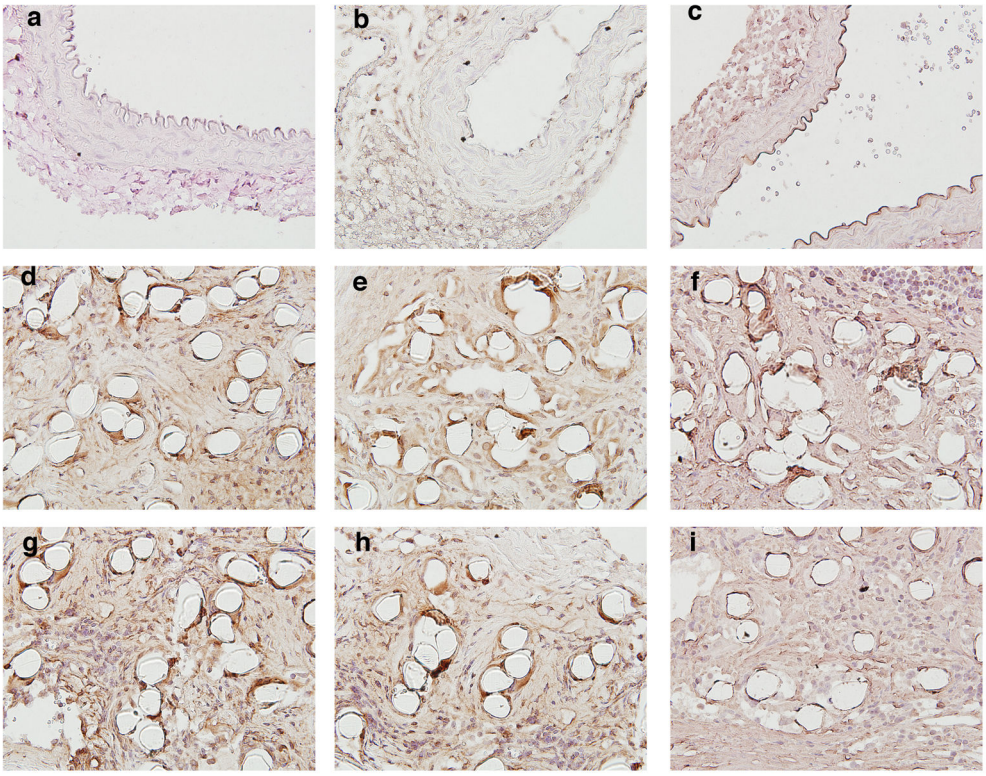

Figure 7.

Evaluation of inflammatory response to TEVG. Native mouse IAA stained for (*a–c*): F4/80 (mouse macrophage marker), MMP-2, and MMP-9. Similarly, TEVG at 3 months (*d–f*) and 7 months (*g–i*) stained for F4/80, MMP-2, and MMP-9. All photomicrographs are at a magnification of 300×.

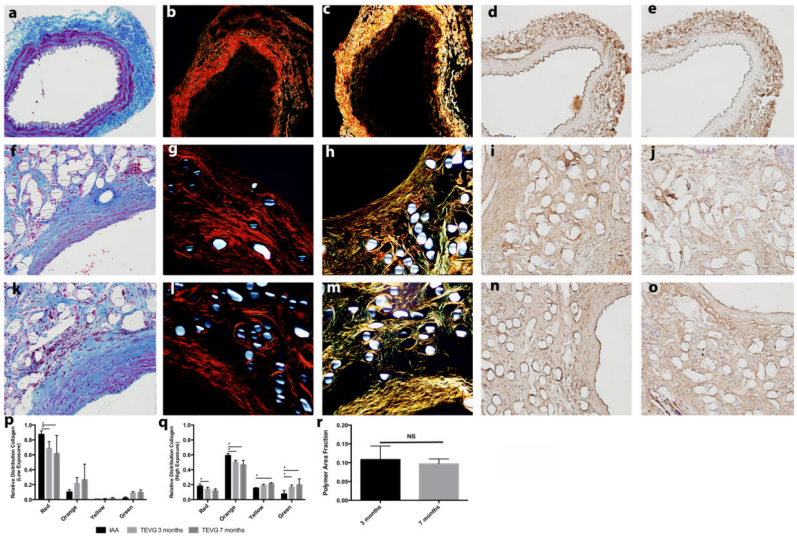

Figure 8.

Evaluation of collagen development within TEVGs. Native mouse IAA stained with (*a–e*): TRI, PSR focused on adventitia (PSR ADV), PSR focused on media (PSR MED), COL I, and COL III. Similarly, TEVG at 3 months (*f–j*) and 7 months (*k–o*) stained for TRI, PSR focused on adventitia (PSR ADV), PSR focused on media (PSR MED), COL I, and COL III. (*p*) Relative percentage of large diameter and small diameter fibers by PSR staining at low light exposure (adventitia). (*q*) Relative percentage of large diameter and small diameter fibers by PSR staining at high light exposure (media). H&E stain under polarized light at (*r*) 3 months and (*s*) 7 months, both at (10×). (*t*) Area fraction of polymer at 3 and 7 months. All photomicrographs at magnification of 200×. Data in graphs are expressed as mean ± SD (n=4 for all groups).

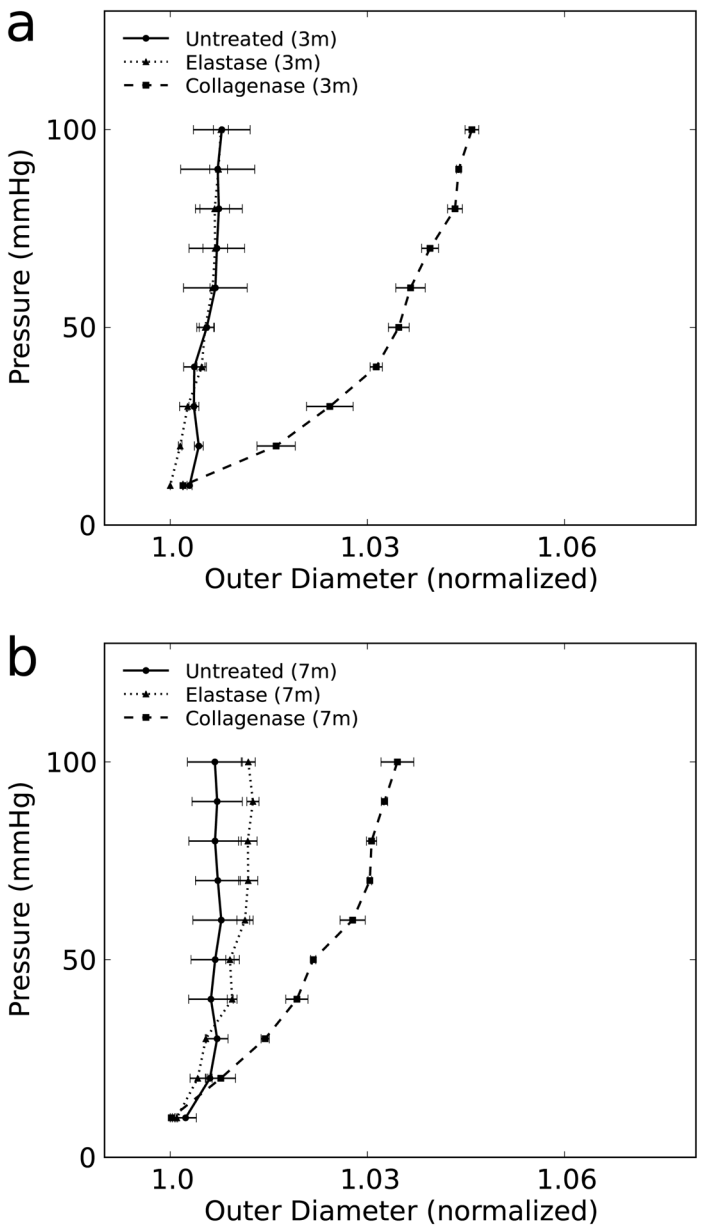

Figure 9.

Pressure-diameter curves for untreated (*n*=4), elastase treated (*n*=2), and partial-collagenase (*n*=2) treated TEVGs at (*a*) 3 months and (*b*) 7 months. Data in graphs are expressed as mean ± SEM.

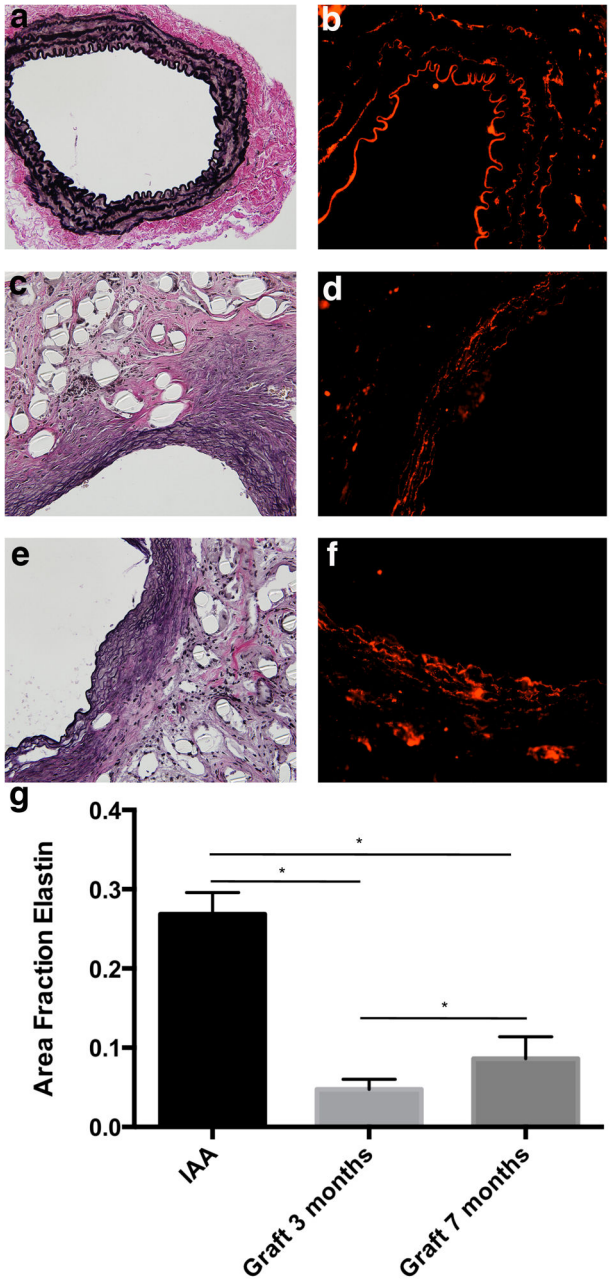

Figure 10.

Evaluation of elastin fiber development within TEVGs. Native mouse IAA stained for (*a* and *b*): VVG (elastic fibers) and TRO. Similarly, TEVG at 3 months (*c* and *d*) and 7 months (*e* and *f*) stained for VVG and TRO. (*g*) Area fraction of elastin within biologically active stained tissue by VVG stain (n=4 for all groups). VVG and TRO photomicrographs are at a magnification of 200× and 300× respectively. Data in graphs are expressed as mean ± SD.

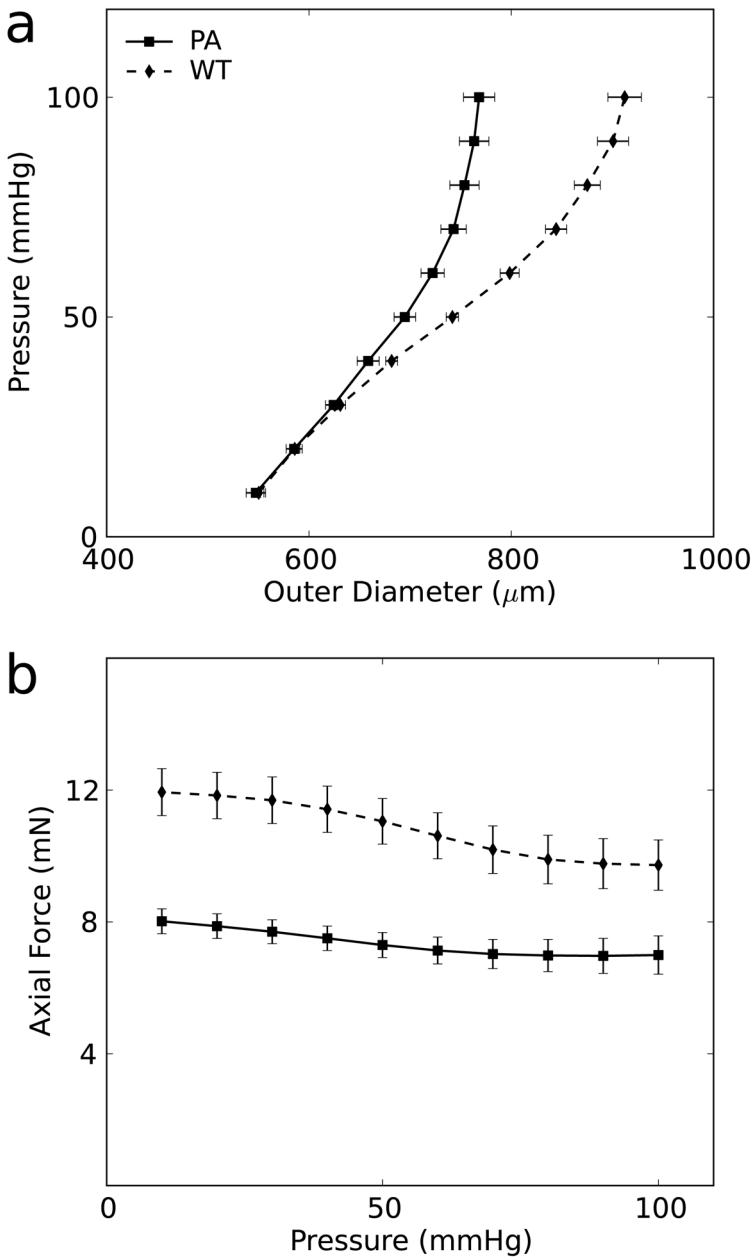

Figure 11.

Comparison of IAA in mice with and without TEVG implant. Pressure diameter curve (*a*) and pressure-force curve (*b*) between non-implanted (WT) mice and proximal IAA (PA) in mice with TEVG implant at 7 months. Non-implanted data adapted with permission from Ferruzzi et al. (Ferruzzi et al., 2013b).